PHYSICAL REVIEW D **87,** 123006 (2013)

Boson stars in AdS spacetime

Alex Buchel,[1,2] Steven L. Liebling,[1,3] and Luis Lehner[1]

[1]*Perimeter Institute for Theoretical Physics, Waterloo, Ontario N2J 2W9, Canada*

[2]*Department of Applied Mathematics, University of Western Ontario, London, Ontario N6A 5B7, Canada*

[3]*Department of Physics, Long Island University, Brookville, New York 11548, USA*

(Received 22 April 2013; published 20 June 2013)

We construct boson stars in global anti–de Sitter (AdS) space and study their stability. Linear perturbation results suggest that the ground state along with the first three excited state boson stars are stable. We evolve some of these solutions and study their nonlinear stability in light of recent work [9], arguing that a weakly turbulent instability drives scalar perturbations of AdS to black hole formation. However, evolutions suggest that boson stars are nonlinearly stable and immune to the instability for sufficiently small perturbation. Furthermore, these studies find other families of initial data which similarly avoid the instability for sufficiently weak parameters. Heuristically, we argue that initial data families with widely distributed mass energy distort the spacetime sufficiently to oppose the coherent amplification favored by the instability. From the dual CFT perspective our findings suggest that there exist families of rather generic initial conditions in strongly coupled CFT (with large number of degrees of freedom) that do not thermalize in the infinite future.

DOI: 10.1103/PhysRevD.87.123006 PACS numbers: 97.60.Lf, 04.20.−q, 11.10.Kk

I. INTRODUCTION

Understanding the gravitational behavior of spacetimes which asymptotically behave as anti–de Sitter (AdS) has, since holography [1], attracted significant interest. The AdS/CFT correspondence conjecture implies that such understanding is critically important for a plethora of phenomena described by field theories. Remarkably, however, relatively little is known about dynamical scenarios, especially in comparison to spacetimes that are asymptotically flat (AF) or asymptotically deSitter (dS). An important reason behind this difference is that the boundary of AdS is in causal contact with the interior of the spacetime, in stark contrast to the boundaries of AF and asymptotically dS spacetimes. That the boundary affects the interior prevents a straightforward extension of standard singularity theorems to asymptotically AdS (aAdS) spacetimes [2].

Significant advances have recently been achieved via different approaches, including strictly analytic [3–6], perturbative [7,8] and numerical [9–15] (to name a few representative) efforts. Particularly intriguing is the evidence first presented in [9] that pure AdS is unstable to scalar collapse to black hole (BH), regardless of how small a scalar perturbation is considered. The effect of the AdS boundary allows for the reflection of scalar pulses. Hence, a weak scalar pulse bounces off the boundary at infinity, returning to concentrate again at the origin. The weakly turbulent instability of [9] results in the sharpening of the pulse so that, eventually, it achieves sufficient concentration to form a black hole. The black hole critical behavior discovered by Choptuik [16] in AF spacetimes appears here repeatedly. In particular, after each reflection off the AdS boundary, there is yet another threshold for prompt BH formation (before the next bounce).

To explain this behavior, a study of the normal modes of scalar [9] and tensor [8] perturbations revealed a nonlinear mode coupling at third order, shifting energy to higher frequencies. Consequently, this shift in frequency would eventually lead to the formation of a black hole and so generic instability of AdS was conjectured. Interestingly, though, further studies suggested the existence of nonlinearly stable solutions [7,13,15,17]. These observations hint that a straightforward application of the resonance picture can only partially capture the dynamical behavior.

We consider the dynamics of boson stars in AdS, motivated towards better understanding of this instability and its implications for holographic scenarios. Horizon formation in gravitational collapse from the holographic perspective implies thermalization of the dual conformal theory. When the gravitational problem is formulated in global $d+1$ spacetime dimensional asymptotically AdS_{d+1}, the dynamics of the dual d spacetime dimensional CFT_d occurs on a S^{d-1} sphere. Furthermore, the holographic duality arises as a correspondence between a string theory and a CFT—it can be truncated to a gravity/CFT duality when a CFT has a large number of strongly interacting degrees of freedom.[1] A natural expectation from the field theory perspective is that a large number of strongly interacting degrees of freedom in a finite volume thermalize from generic initial conditions; thus, one does expect no-threshold BH formation as advocated in [9]. Early work on boson stars in AdS [18] demonstrated that such stationary configurations are linearly stable. Thus, initializing

[1]This can be quantified as a large central charge for even d, or more generically, the large number of excited degrees of freedom at thermal equilibrium.

a CFT state as a dual to an AdS boson star might result in a slow thermalization of the latter.

In this paper we show, rather, that boson stars in AdS are non-linearly stable. This nonlinear stability is unaffected by boson star perturbations, as long as these perturbations are sufficiently small. Even more surprising, we find that families of initial conditions with widely distributed mass energy are nonlinearly stable for sufficiently small mass as well. This suggests that nonlinear stability is not a feature of states carrying a global charge (as dual to boson stars). As a result, it appears that there exist large sets of initial configurations in CFT which never thermalize in their evolution.

The paper is organized as follows. In Sec. II we set up the gravitational dual of the generic, spatially isotropic CFT_3, initial condition specified by a pair of dimension-three operators with a global $U(1)$ symmetry: an Einstein gravity with a negative cosmological constant and a massless, minimally coupled bulk complex scalar field. In Sec. III we construct stationary configurations of the coupled scalar-gravity system, charged under the global $U(1)$ symmetry—boson stars. We show that boson stars are stable under linearized fluctuations. In Sec. IV we present results of fully nonlinear simulations of genuine boson stars, perturbed boson stars, and $U(1)$-neutral initial configurations with widely distributed, bulk mass energy. We conclude in Sec. V and outline future directions.

II. EFFECTIVE ACTION AND EQUATIONS OF MOTION

In this section, following [13], we review the formulation of the problem of the gravitational collapse of a complex scalar in asymptotically anti–de Sitter spacetime. We focus on asymptotically AdS_4 collapse, dual to CFT_3 (we choose $d = 3$ in the notation of [13]).

The effective four-dimensional action is given by[2]

$$S_4 = \frac{1}{16\pi G_4}\int_{\mathcal{M}_4} d^4\xi\sqrt{-g}(R_4 + 6 - 2\partial_\mu\phi\partial^\mu\phi^*), \quad (2.1)$$

where $\phi \equiv \phi_1 + i\phi_2$ is a complex scalar field and

$$\mathcal{M}_4 = \partial\mathcal{M}_3 \times I, \quad \partial\mathcal{M}_3 = R_t \times S^2, \quad I = \left\{x \in \left[0, \frac{\pi}{2}\right]\right\}. \quad (2.2)$$

Adopting the line element as in [19],

$$ds^2 = \frac{1}{\cos^2 x}\left(-Ae^{-2\delta}dt^2 + \frac{dx^2}{A} + \sin^2 x d\Omega_2^2\right), \quad (2.3)$$

where $d\Omega_2^2$ is the metric of unit radius S^2, and $A(x, t)$ and $\delta(x, t)$ are scalar functions describing the metric. Rescaling the matter fields as in [13]

$$\hat{\phi}_i \equiv \frac{\phi_i}{\cos^2 x}, \quad (2.4)$$

$$\hat{\Pi}_i \equiv \frac{e^\delta}{A}\frac{\partial_t\phi_i}{\cos^2 x}, \quad (2.5)$$

$$\hat{\Phi}_i \equiv \frac{\partial_x\phi_i}{\cos x}, \quad (2.6)$$

we find the following equations of motion (we drop the caret from here forward):

$$\dot{\phi}_i = Ae^{-\delta}\Pi_i, \qquad \dot{\Phi}_i = \frac{1}{\cos x}(\cos^2 x Ae^{-\delta}\Pi_i)_{,x},$$
$$\dot{\Pi}_i = \frac{1}{\sin^2 x}\left(\frac{\sin^2 x}{\cos x}Ae^{-\delta}\Phi_i\right)_{,x}. \quad (2.7)$$

$$A_{,x} = \frac{1 + 2\sin^2 x}{\sin x\cos x}(1 - A) - \sin x\cos^5 x A\left(\frac{\Phi_i^2}{\cos^2 x} + \Pi_i^2\right),$$
$$\delta_{,x} = -\sin x\cos^5 x\left(\frac{\Phi_i^2}{\cos^2 x} + \Pi_i^2\right), \quad (2.8)$$

together with one constraint equation,

$$A_{,t} + 2\sin x\cos^4 x A^2 e^{-\delta}(\Phi_i\Pi_i) = 0, \quad (2.9)$$

where a sum over $i = \{1, 2\}$ is implied. We are interested in studying the solution to (2.7), (2.8), and (2.9) subject to the following boundary conditions:

(i) regularity at the origin implies these quantities behave as

$$\phi_i(t, x) = \phi_0^{(i)}(t) + \mathcal{O}(x^2), \qquad A(t, x) = 1 + \mathcal{O}(x^2),$$
$$\delta(t, x) = \delta_0(t) + \mathcal{O}(x^2) \quad (2.10)$$

(ii) at the outer boundary, $x = \pi/2$, we introduce $\rho \equiv \pi/2 - x$ so that we have

$$\phi_i(t, \rho) = \phi_3^{(i)}(t)\rho + \mathcal{O}(\rho^3),$$
$$A(t, \rho) = 1 - M\frac{\sin^3\rho}{\cos\rho} + \mathcal{O}(\rho^6), \quad (2.11)$$
$$\delta(t, \rho) = 0 + \mathcal{O}(\rho^6).$$

The asymptotic behavior (2.11) determines the following boundary CFT observables: the expectation values of the stress-energy tensor T_{kl}, and the operators $\mathcal{O}_3^{(i)}$, dual to ϕ_i:

$$8\pi G_4\langle T_{tt}\rangle = M, \qquad \langle T_{\alpha\beta}\rangle = \frac{g_{\alpha\beta}}{2}\langle T_{tt}\rangle,$$
$$16\pi G_{d+1}\langle\mathcal{O}_3^{(i)}\rangle = 12\phi_3^{(i)}(t), \quad (2.12)$$

where $g_{\alpha\beta}$ is a metric on a round S^2. Additionally note that the conserved $U(1)$ charge is given by

[2]We set the radius of AdS to one.

$$Q = 8\pi \int_0^{\pi/2} dx \sin^2 x \cos^2 x (\Pi_2(0,x)\phi_1(0,x) - \Pi_1(0,x)\phi_2(0,x)), \tag{2.13}$$

and that since $\partial_t Q = 0$, the integral in (2.13) can be evaluated at $t = 0$.

The constraint (2.9) implies that M in (2.11) is time independent, ensuring energy conservation,

$$\partial_t \langle T_{tt} \rangle = 0. \tag{2.14}$$

It is convenient to introduce the mass aspect function $\mathcal{M}(t,x)$ as

$$A(t,x) = 1 - \mathcal{M}(t,x)\frac{\cos^3 x}{\sin x}. \tag{2.15}$$

Following (2.8) we find

$$\mathcal{M}(t,x) = \int_0^x dz \tan^2 z \cos^4 z A(t,z)\left[\frac{\Phi_i^2(t,z)}{\cos^2 z} + \Pi_i^2(t,z)\right]. \tag{2.16}$$

Comparing (2.16) and (2.11) we see that

$$M = \mathcal{M}(t,x)|_{x=\frac{\pi}{2}}. \tag{2.17}$$

III. BOSON STARS IN AdS$_4$

There is an interesting class of stationary, perturbatively stable, fully nonlinear solutions to (2.7), (2.8), (2.9), (2.10), and (2.11) with nonzero Q, referred to as boson stars [18,20]. Such solutions are characterized by a discrete integer $n = 0, 1, \ldots$, denoting the number of nodes of the complex scalar radial wave function and a continuous value of the global charge Q. In this section we discuss the numerical construction of such solutions, their perturbative properties, linearized stability, and their relation (for small Q) to linearized AdS$_4$ massless, minimally coupled, scalar modes—the oscillons. Oscillons were reviewed in detail in [13]. These stationary solutions are uniquely characterized by an excitation level $j = \{0, 1, \ldots\}$,

$$e_j(x) = d_j \cos^3 x \, {}_2F_1\left(-j, 3+j; \frac{3}{2}; \sin^2 x\right),$$
$$w^{(j)} = 3 + 2j, \qquad d_j = \left(\frac{16(j+1)(j+2)}{\pi}\right)^{1/2}, \tag{3.1}$$

where $w^{(j)}$ is an oscillon frequency and d_j is a constant enforcing their orthonormality,

$$\int_0^{\pi/2} dx e_i(x) e_j(x) \tan^2 x = \delta_{ij}. \tag{3.2}$$

A. Stationary boson stars

Assuming a stationary solution in which the complex field varies harmonically,

$$\phi_1(x,t) + i\phi_2(x,t) = \frac{\phi(x)}{\cos^2 x} e^{i\omega t}, \qquad A(t,x) = a(x), \qquad \delta(t,x) = d(x), \tag{3.3}$$

we find a system of ordinary differential equations from (2.7) and (2.8),

$$\begin{aligned} 0 &= \phi'' + \left(\frac{2}{\cos x \sin x} + \frac{a'}{a} - d'\right)\phi' + \omega^2 e^{2d} a^{-2}\phi, \\ 0 &= d' + \sin x \cos x a^{-2}((\phi')^2 a^2 + \phi^2 \omega^2 e^{2d}), \\ 0 &= a' + \frac{2\cos^2 x - 3}{\cos x \sin x}(1-a) \\ &\quad + \sin x \cos x a^{-1}((\phi')^2 a^2 + \phi^2 \omega^2 e^{2d}). \end{aligned} \tag{3.4}$$

The charge and the mass determined by these solutions are given by

$$\begin{aligned} Q &= 8\pi \int_0^{\pi/2} dx \frac{\omega \sin^2 x \phi(x)^2 e^{d(x)}}{a(x)\cos^2 x}, \\ M &= \int_0^{\pi/2} dx \frac{\sin^2 x}{a(x)\cos^2 x}(a(x)^2(\phi'(x))^2 + e^{2d(x)}\omega^2\phi(x)^2). \end{aligned} \tag{3.5}$$

A physically relevant solution to Eq. (3.4) must satisfy

(i) at the origin of AdS, i.e., $x \to 0$,

$$\begin{aligned} a &= 1 - \frac{1}{3}(p_0^h)^2 \omega^2 e^{2d_0^h} x^2 + \mathcal{O}(x^4), \\ d &= d_0^h - \frac{1}{2}(p_0^h)^2 \omega^2 e^{2d_0^h} x^2 + \mathcal{O}(x^4), \\ \phi &= p_0^h - \frac{1}{6} p_0^h \omega^2 e^{2d_0^h} x^2 + \mathcal{O}(x^4). \end{aligned} \tag{3.6}$$

Note that besides ω, the general solution is characterized by

$$\{p_0^h, d_0^h\}. \tag{3.7}$$

(ii) and asymptotically (at the AdS boundary, i.e., $\rho \to 0$),

$$\begin{aligned} a &= 1 + a_3^b \rho^3 + \mathcal{O}(\rho^6), \\ d &= \frac{3}{2}(p_3^b)^2 \rho^6 + \left(\frac{3}{4}(p_3^b)^2 - \frac{1}{4}(p_3^b)^2\omega^2\right)\rho^8 + \mathcal{O}(\rho^9), \\ \phi &= p_3^b \rho^3 + \left(\frac{2}{5}p_3^b - \frac{1}{10}p_3^b\omega^2\right)\rho^5 + \mathcal{O}(\rho^6). \end{aligned} \tag{3.8}$$

Note that besides ω, the general solution is characterized by

$$\{p_3^b, a_3^b\}. \tag{3.9}$$

From (3.7) and (3.9) we have precisely the correct number of coefficients to find an isolated solution[3] for a given ω.

[3] As we discuss in Sec. III B, solutions of a fixed charge are labeled by an integer, specifying the "level" of a boson star.

B. Small charge boson stars as oscillons

In this section we discuss analytic results for the spectrum of boson stars perturbatively in the amplitude ϕ. To this end we introduce

$$\begin{aligned} &\phi = \lambda\phi_1 + \mathcal{O}(\lambda^3), \quad a = 1 + \lambda^2 a_2 + \mathcal{O}(\lambda^4), \\ &e^d = 1 + \lambda^2 d_2 + \mathcal{O}(\lambda^4), \quad \omega = \omega_0 + \omega_2\lambda^2 + \mathcal{O}(\lambda^4), \end{aligned} \tag{3.10}$$

where λ is an expansion parameter. Substituting (3.10) into (3.4), we find that the equation for ϕ_1 decouples to leading order,

$$0 = \phi_1'' + \frac{2}{\sin x \cos x}\phi_1' + \omega_0^2\phi_1. \tag{3.11}$$

Normalizing ϕ_1 as

$$\phi_1|_{x\to 0_+} = 1, \tag{3.12}$$

the general solution of (3.11), subject to the boundary conditions (3.6) and (3.8), is given by

$$\phi_1^{(j)} = \frac{1}{d_j}e_j(x), \qquad \omega_0^{(j)} = w^{(j)} = 3 + 2j, \tag{3.13}$$

where the integer $j = 0, 1, 2\ldots$ parametrizes the "excitation level" of the boson star. Notice that the asymptotic expansion for ϕ [in Eq. (3.6)] implies $p_0^h = \lambda$. Given (3.13), we find from (3.5),

$$\begin{aligned} M &= \lambda^2\frac{\pi(3+2j)^2}{8(j+1)(j+2)} + \mathcal{O}(\lambda^4), \\ Q &= \lambda^2\frac{\pi^2(3+2j)}{2(j+1)(j+2)} + \mathcal{O}(\lambda^4), \\ M &= \frac{3+2j}{4\pi}Q + \mathcal{O}(Q^2) = \frac{\omega_0^{(j)}}{4\pi}Q + \mathcal{O}(Q^2). \end{aligned} \tag{3.14}$$

Note from (3.14) that for a fixed charge Q, excited levels of boson stars are more massive.

It is straightforward to compute the leading-order background warp factors $\{a_2, d_2\}$, as well as subleading frequency correction ω_2. In what follows we present explicit expressions for the first four levels of a boson star:

(i) $j = 0$ level,

$$a_2^{(0)} = \frac{9\cos^3 x}{8\sin x}\left(\frac{1}{4}\sin(4x) - x\right), \tag{3.15}$$

$$d_2^{(0)} = \frac{3}{2}\cos^6 x, \tag{3.16}$$

$$\omega_2^{(0)} = -\frac{63}{32} \tag{3.17}$$

(ii) $j = 1$ level,

$$a_2^{(1)} = \frac{25\cos^3 x}{72\sin x}\left(\frac{1}{4}\sin(4x)(2\cos(4x)+1) - 3x\right), \tag{3.18}$$

$$d_2^{(1)} = \frac{5}{18}\cos^6 x(32\cos^4 x - 40\cos^2 x + 15), \tag{3.19}$$

$$\omega_2^{(1)} = -\frac{3025}{864} \tag{3.20}$$

(iii) $j = 2$ level,

$$a_2^{(2)} = \frac{49\cos^3 x}{144\sin x}\left(\frac{1}{8}\sin(8x)(2\cos(4x)+1) - 3x\right), \tag{3.21}$$

$$\begin{aligned} d_2^{(2)} = \frac{7}{90}\cos^6 x(&960\cos^8 x - 2240\cos^6 x \\ &+ 1904\cos^4 x - 700\cos^2 x + 105), \end{aligned} \tag{3.22}$$

$$w_2^{(2)} = -\frac{89327}{17280} \tag{3.23}$$

(iv) $j = 3$ level,

$$\begin{aligned} a_2^{(3)} = \frac{81\cos^3 x}{400\sin x}\Big(&\frac{1}{8}\sin(8x)(2\cos(8x) \\ &+ 2\cos(4x) + 1) - 5x\Big), \end{aligned} \tag{3.24}$$

$$\begin{aligned} d_2^{(3)} = \frac{9}{350}\cos^6 x(&28672\cos^{12} x - 96768\cos^{10} x \\ &+ 130752\cos^8 x - 90048\cos^6 x + 33264\cos^4 x \\ &- 6300\cos^2 x + 525), \end{aligned} \tag{3.25}$$

$$\omega_2^{(3)} = -\frac{154143}{22400}. \tag{3.26}$$

Further comparing the above with (3.6) and (3.8), we identify the condensates perturbatively in $p_0^h = \lambda$ (see Table I).

C. Numerical boson stars

In the previous section we identified the first four levels of a boson star perturbatively in the amplitude p_0^h. Here we report results for $\{\omega, d_0^h, p_3^b, d_3^b\}$, as well as $\{M, Q\}$, for generic p_0^h from the numerical solution of (3.4). These results are collected in Figs. 1 and 2.

TABLE I. Condensate values (3.6) and (3.8) of boson stars, perturbatively in $p_0^h = \lambda$.

j	$\frac{\omega-\omega_0^{(j)}}{\lambda^2} + \mathcal{O}(\lambda^2)$	$\frac{d_0^h}{\lambda^2} + \mathcal{O}(\lambda^2)$	$\frac{p_3^b}{\lambda} + \mathcal{O}(\lambda^2)$	$\frac{a_3^b}{\lambda^2} + \mathcal{O}(\lambda^2)$
0	$-\frac{63}{32}$	$\frac{3}{2}$	1	$-\frac{9}{16}\pi$
1	$-\frac{3025}{864}$	$\frac{35}{18}$	$-\frac{5}{3}$	$-\frac{25}{48}\pi$
2	$-\frac{89327}{17280}$	$\frac{203}{90}$	$\frac{7}{3}$	$-\frac{49}{96}\pi$
3	$-\frac{154143}{22400}$	$\frac{873}{350}$	-3	$-\frac{81}{160}\pi$

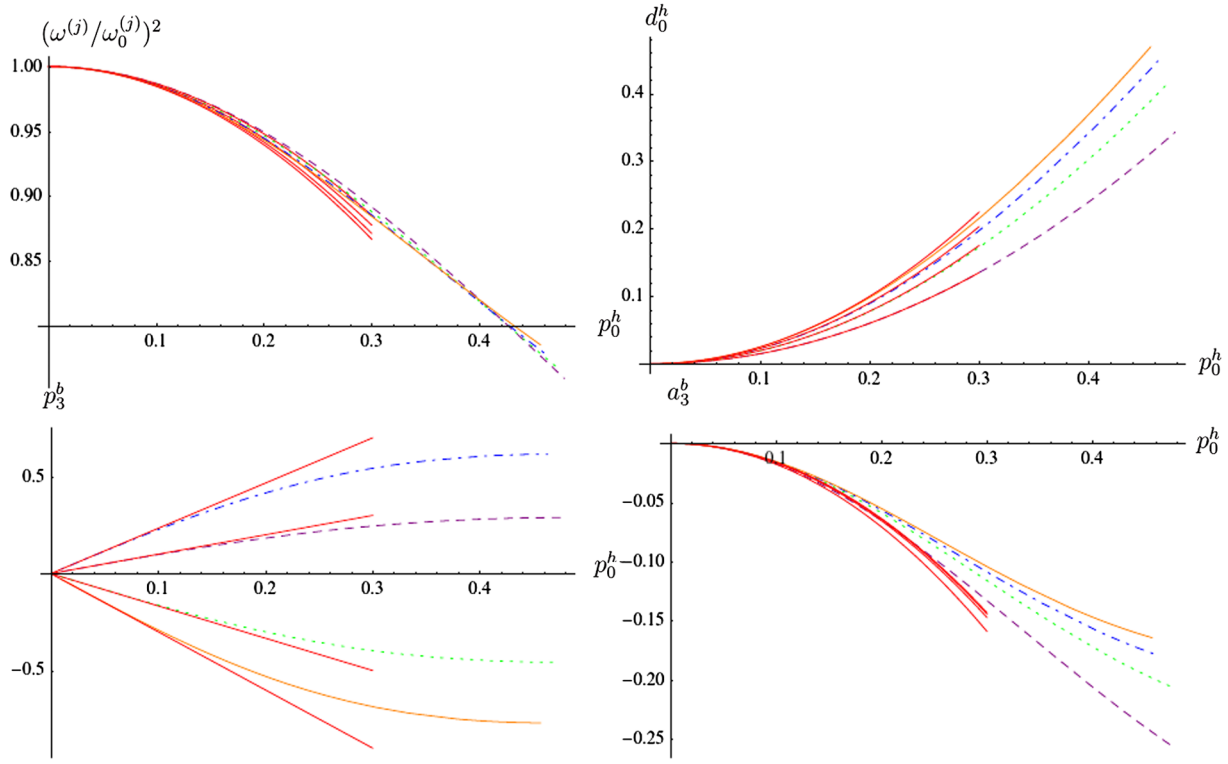

FIG. 1 (color online). Condensate values (3.6) and (3.8) for level $j = \{0, 1, 2, 3\}$ (dashed purple, dotted green, dot-dashed blue, solid orange curves) boson stars. The red lines represent perturbative in p_0^h approximations, see Table I.

The top-left panel of Fig. 1 presents the frequency $\omega^{(j)}$ of a level-j boson star rescaled to that of a level-j oscillon frequency $\omega_0^{(j)}$ [see (3.13)]. We use purple/green/blue/orange color coding to denote $j = 0 \ldots 3$. As p_0^h (and correspondingly the mass and the charge—see Fig. 2) of a boson star grows, its frequency decreases. The remaining panels in Fig. 1 present the dependence of $\{d_0^h, p_3^b, d_3^b\}$ as a function of p_0^h. Notice that p_3^b saturates; this saturation is the main obstacle in generating boson stars with ever increasing values of p_0^h (or mass). The red curves indicate perturbative approximations in p_0^h as collected in Table I, (Fig. 1), and perturbative approximation (3.14) in Q (right panel of Fig. 2).

In the limit of vanishing charge Q, the level-j boson star radial profile $\phi^{(j)}$ is a single level-j oscillon [see (3.13) and (3.14)],

$$\phi^{(j)}(x) \propto \sqrt{Q} e_j(x). \tag{3.27}$$

For finite Q all the oscillons are excited. In Fig. 3 we present the spectral decomposition in the oscillon basis of the most massive level-j boson stars that we were able to construct,

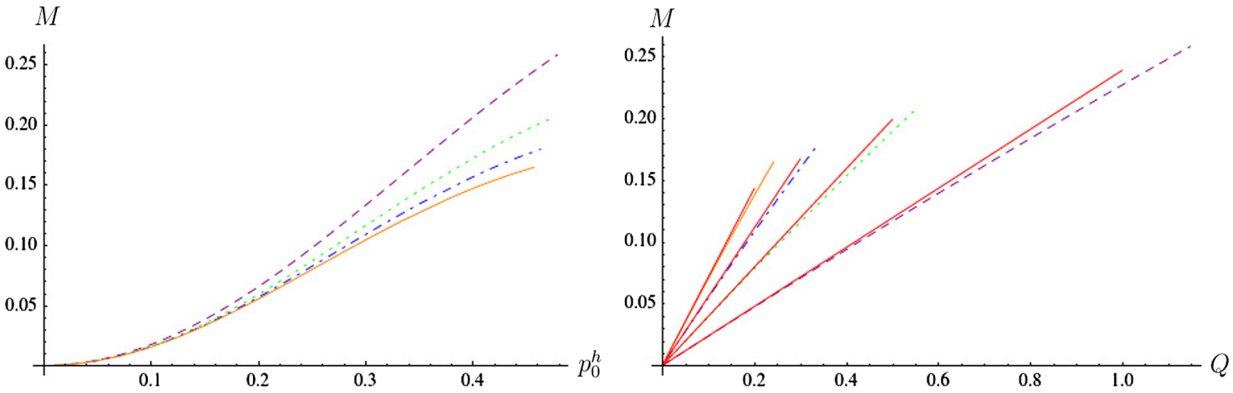

FIG. 2 (color online). Mass vs p_0^h (left panel) and vs charge (right panel) for level $j = \{0, 1, 2, 3\}$ (dashed purple, dotted green, dot-dashed blue, solid orange curves) boson stars. The red lines represent perturbative in Q approximations, see (3.14).

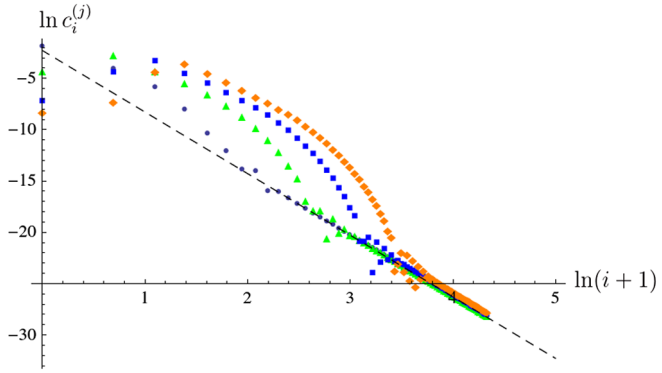

FIG. 3 (color online). Spectral decomposition of level $j = \{0, 1, 2, 3\}$ (purple circles, green triangles, blue squares, orange diamonds boson stars in oscillon basis, see (3.29). For large i all the curves approach a universal falloff $c_i^{(j)} \propto (1+i)^{-6}$ (the black dashed curve).

$$c_i^{(j)} \equiv \left| \int_0^{\pi/2} dx \phi^{(j)}(x) e_i(x) \tan^2 x \right|. \tag{3.28}$$

Note that the maxima of $c_i^{(j)}$ are achieved for $i = j$, much like in the small-Q limit. For all levels considered, $c_i^{(j)}$ approach a universal fall-off:

$$c_i^{(j)} \propto (1+i)^{-6}, \qquad i \gg j, \tag{3.29}$$

represented by a dashed black curve in Fig. 3.

D. Perturbative stability of boson stars

In this section we explore the linearized stability of boson stars. Consider the following perturbations of stationary solutions (3.3) to leading order in ϵ:

$$\begin{aligned} \phi_1(x,t) + i\phi_2(x,t) &= \cos^{-2} x(\phi(x) \\ &\quad + \epsilon(f_1(t,x) - i\phi(x) g_1(t,x)))e^{i\omega t}, \\ A(t,x) &= a(x) + \epsilon a_1(t,x), \\ \delta(t,x) &= d(x) + \epsilon \delta_1(t,x). \end{aligned} \tag{3.30}$$

Further introducing

$$f_1(t,x) = F_1(x)\cos(\chi t), \qquad g_1(t,x) = -G_1(x)\sin(\chi t), \tag{3.31}$$

the equations for $a_1(t,x)$ and $\delta_1(t,x)$ can be solved explicitly,

$$a_1(t,x) = \sin(2x) a(x) (\omega \phi(x)^2 G_1'(x) - \phi'(x) F_1(x)) \cos(\chi t), \tag{3.32}$$

$$\begin{aligned} \delta_1(t,x) = &- \frac{e^{-2d(x)}}{\cos(x)\phi(x)\omega \sin(x)} (a(x)^2 \cos(x)\phi(x) G_1''(x) \sin(x) + (-2\cos(x)^2 \phi(x)^3 e^{2d(x)} \sin(x)^2 \omega^2 \\ &+ a(x)(2a(x)\cos(x)\phi'(x)\sin(x) + 2a(x)\cos(x)^2\phi(x) - a(x)\phi(x) - 2\cos(x)^2\phi(x) + 3\phi(x)))G_1'(x) \\ &+ \cos(x)\phi(x) e^{2d(x)} G_1(x) \chi^2 \sin(x) - 2\cos(x) F(x)(\cos(x)^3 \phi(x)\phi'(x) - \cos(x)\phi(x)\phi'(x) \\ &- \sin(x))\omega e^{2d(x)}) \cos(\chi t), \end{aligned} \tag{3.33}$$

where $F_1(x)$ and $G_1(x)$ satisfy a coupled system of equations

$$\begin{aligned} 0 = &F_1'' + \frac{-2\cos(x)^2 + 2\cos(x)^2 a + 3 - a}{a \sin(x)\cos(x)} F_1' - 2\phi\omega G_1'' + \frac{2\omega}{a\sin(x)\cos(x)} (2\sin(x)\phi^2\phi'\cos(x)^3 + 2\cos(x)^2\phi \\ &- 2a\phi\cos(x)^2 - 2\sin(x)a\phi'\cos(x) - 3\sin(x)\phi^2\phi'\cos(x) + a\phi - 3\phi)G_1' \\ &- (4a\cos(x)^2(\phi')^2 - e^{2d}\chi^2 - 6(\phi')^2 a + 3e^{2d}\omega^2)a^{-2}F_1, \end{aligned} \tag{3.34}$$

$$\begin{aligned} 0 = &G_1''' + (-6\cos(x)^2\phi + 6a\phi\cos(x)^2 + 2\sin(x)a\phi'\cos(x) + 9\phi - 7a\phi)(a\phi\sin(x)\cos(x))^{-1} G_1'' \\ &+ (5a^3\phi^2 + 4a^3\sin(x)\phi'\phi\cos(x)^3 - 10a^3\sin(x)\phi'\phi\cos(x) - 4a^2\sin(x)\phi'\phi\cos(x)^3 \\ &+ 6a^2\sin(x)\phi'\phi\cos(x) + 2e^{2d}a\phi^2\omega^2\cos(x)^4 - e^{2d}a\cos(x)^4\phi^2\chi^2 - 2e^{2d}a\phi^2\omega^2\cos(x)^2 \\ &+ e^{2d}a\cos(x)^2\phi^2\chi^2 + 2a^2(\phi')^2\cos(x)^6\phi^2 - 5a^2(\phi')^2\cos(x)^4\phi^2 + 3a^2(\phi')^2\cos(x)^2\phi^2 + 9e^{2d}\cos(x)^2\phi^4\omega^2 \\ &+ 6e^{2d}\cos(x)^6\phi^4\omega^2 - 15e^{2d}\cos(x)^4\phi^4\omega^2 - 16a^3\phi^2\cos(x)^2 + 8a^3\phi^2\cos(x)^4 + 9a\phi^2 - 12a^2\phi^2 \\ &+ 24a^2\cos(x)^2\phi^2 - 12a^2\cos(x)^4\phi^2 - 12a\cos(x)^2\phi^2 + 4a\cos(x)^4\phi^2 + 2a^3(\phi')^2\cos(x)^4 \\ &- 2a^3(\phi')^2\cos(x)^2)(a^3\phi^2\sin(x)^2\cos(x)^2)^{-1} G_1' + \frac{2e^{2d}\omega}{a^2\phi} F_1' + (4\phi^2\cos(x)^2 - 2a - 6\phi^2)e^{2d}\omega\phi'(a^3\phi^2)^{-1} F_1. \end{aligned} \tag{3.35}$$

Notice that (3.34) and (3.35) are left invariant under the shift

$$G_1 \to G_1 + \mathcal{G}, \tag{3.36}$$

where $\mathcal{G}$ is an arbitrary constant. From (3.33) is it clear that this constant is fixed uniquely requiring that

$$\lim_{x\to\pi/2} \delta_1(t, x) = 0, \tag{3.37}$$

i.e., we keep the time coordinate at the boundary fixed. We do not have to worry about the shift symmetry (3.36), provided we rewrite (3.34) and (3.35) using

$$dG_1(x) \equiv G_1'(x). \tag{3.38}$$

Equations (3.34) and (3.35) must be solved subject to constraints that $F_1(x)$ and $G_1(x)\phi(x)$ are regular for $x \in [0, \pi/2)$ and have only normalizable modes as $x \to \pi/2$, i.e.,

$$F_1 \propto \rho^3, \qquad G_1 \propto \text{const}, \quad \text{as } \rho \to 0. \tag{3.39}$$

The latter regularity condition implies that G_1 can have a simple pole (or dG_1 can have a double pole) precisely where $\phi(x)$ has a zero.[4] These poles represent a technical difficulty in identifying the fluctuations about excited boson stars—specifically, a straightforward shooting method: integrating from both boundaries with suitable boundary conditions and demanding continuity at an arbitrary radial location will invariably encounter these poles rendering this method delicate to apply.

Here we discuss the fluctuations about the lowest-level (ground state) boson stars and also present analytic results for fluctuations about perturbatively light excited boson stars.[5]

Finally, since the system of equations (3.34) and (3.35) is linear, we can further fix the normalizable mode F_1,

$$\lim_{\rho\to 0} \frac{F_1}{\rho^3} = 1. \tag{3.40}$$

Given (3.39) and (3.40), we can specify the following boundary conditions for $\{dG_1, F_1\}$:

(i) at the origin of AdS, i.e., as $x \to 0$,

$$dG_1 = 2g_1^h x + \mathcal{O}(x^3), \qquad F_1 = f_0^h + \mathcal{O}(x^2) \tag{3.41}$$

(ii) at the AdS boundary, i.e., as $\rho \to 0$

$$dG_1 = 2g_2^b \rho + \mathcal{O}(\rho^3), \qquad F_1 = \rho^3 + \mathcal{O}(\rho^5). \tag{3.42}$$

[4]Recall that excited level stationary boson stars are characterized by the number of nodes in the radial profile $\phi(x)$, see (3.3).

[5]We verified explicitly that while $dG_1^{(1)}$ to order $\mathcal{O}(\lambda^3)$ has a double pole at the location of the zero of $\phi^{(1)}$ [constructed perturbatively in λ to order $\mathcal{O}(\lambda^5)$ inclusive, see (3.10)], the full radial profile of physical fluctuations, $G_1^{(1)}\phi^{(1)}$, is smooth for $x \in [0, \pi/2]$.

Note that along with χ, the physical solution $\{dG_1, F_1\}$ is characterized by $\{g_1^h, f_0^h, g_2^b\}$, which is the correct number of coefficients necessary to determine a unique (or isolated) solution for a pair of coupled second-order ordinary differential equations (3.34) and (3.35).

Using the boundary conditions (3.41) and (3.42), it is easy to see that the charge of a fluctuating boson star does not change to leading order in ϵ,

$$\delta Q \propto \int_0^{\pi/2} dx \frac{d}{dx}\left\{\frac{\sin(x)^2\phi(x)^2 a(x) G_1'(x)}{e^{d(x)}\cos(x)^2}\right\} = 0. \tag{3.43}$$

1. Linearized fluctuations about light boson stars

We report here the results for solving (3.34) and (3.35) for light boson stars, i.e., perturbatively in λ, see Sec. III B. In general, we search solutions to the above equations as a series,

$$\begin{aligned} dG_1^{(j)}(x) &= \lambda dG_{1,1}^{(j)} + \lambda^3 dG_{1,3}^{(j)} + \mathcal{O}(\lambda^5), \\ F_1^{(j)} &= F_{1.0}^{(j)} + \lambda^2 F_{1,2}^{(j)} + \lambda^4 F_{1,4}^{(j)} + \mathcal{O}(\lambda^6), \\ \chi^{(j)} &= \chi_0^{(j)} + \lambda^2 \chi_1^{(j)} + \lambda^4 \chi_2^{(j)} + \mathcal{O}(\lambda^6), \end{aligned} \tag{3.44}$$

where j is the excitation level of a boson star.

We find[6]

(i) $j = 0$ level,

$$\begin{aligned} \chi_0^{(0)} &= 6, \qquad \chi_1^{(0)} = -\frac{135}{32}, \\ \chi_2^{(0)} &= \frac{1215}{128}\pi^2 - \frac{113892831}{1254400}, \end{aligned} \tag{3.45}$$

$$F_{1,0}^{(0)} = \cos^3 x, \tag{3.46}$$

$$\begin{aligned} F_{1,2}^{(0)} = &\frac{\cos(x)^3}{4480\sin(x)}(5760\cos(x)^8\sin(x) \\ &- 14896\cos(x)^6\sin(x) + 18738\cos(x)^4\sin(x) \\ &+ 7560\cos(x)^3 x - 9153\cos(x)^2\sin(x) \\ &- 15120x\cos(x) + 1890\sin(x)\pi^2 - 7560x^2\sin(x)) \\ &- 2\cos(x)^5(32\cos(x)^4 - 54\cos(x)^2 + 27)\mathcal{C}_{1,1}, \end{aligned} \tag{3.47}$$

[6]For excited levels we present only the coefficients $\{\chi_i^{(j)}\}$, $i = 0, 1$, $j = 1 \cdots 3$.

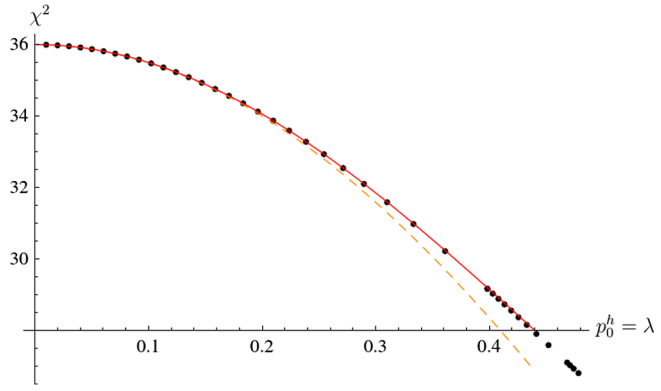

FIG. 4 (color online). Spectrum of linearized fluctuations about $j = 0$ boson stars as a function of p_0^h (black dots). The dashed orange/solid red curves are successive approximations to $\chi^2 = (\chi(p_0^h \equiv \lambda))^2$ in λ^2, see (3.44).

$$dG_{1,1}^{(0)} = -\frac{1}{4480}\sin(x)\cos(x)(5760\cos(x)^6 - 9376\cos(x)^4 + 9900\cos(x)^2 - 2799) + 2\sin(x)\cos(x)(8\cos(x)^2 - 3) \times (4\cos(x)^2 - 3)\mathcal{C}_{1,1}. \tag{3.48}$$

The integration constant $\mathcal{C}_{1,1}$ is not fixed at order $\mathcal{O}(\lambda^2)$, but is uniquely determined[7] at order $\mathcal{O}(\lambda^4)$,

$$\mathcal{C}_{1,1} = \frac{3163}{421120}. \tag{3.49}$$

(ii) $j = 1$ level,

$$\chi_0^{(1)} = 10, \qquad \chi_1^{(1)} = -\frac{2075}{288}. \tag{3.50}$$

(iii) $j = 2$ level,

$$\chi_0^{(2)} = 14, \qquad \chi_1^{(2)} = -\frac{60613}{5760}. \tag{3.51}$$

(iv) $j = 3$ level,

$$\chi_0^{(3)} = 18, \qquad \chi_1^{(3)} = -\frac{62451}{4480}. \tag{3.52}$$

E. Linearized fluctuations about $j = 0$ boson stars

The spectrum of linearized fluctuations about $j = 0$ boson stars is presented in Fig. 4. We find that over the whole range of charges Q, we were able to construct $j = 0$ boson stars, the frequency of their fluctuations squared (χ^2) is positive. This strongly suggests that the ground state boson stars are perturbatively stable.

[7]This pattern extends to higher orders in λ: a solution at order λ^{2n}, $\{F_{1,2n}, G_{1,2n-1}\}$, is determined up to a constant $\mathcal{C}_{1,n}$, which is being uniquely fixed at order $\mathcal{O}(\lambda^{2(n+1)})$.

As discussed in the previous section [see (3.50), (3.51), and (3.52)], excited boson stars are perturbatively stable for small charge. Our numerical simulations suggest that both the $j = 0$ and the excited boson stars are nonlinearly stable.

IV. NONLINEAR RESULTS

We take the constructed boson star solutions described above $\{\phi(x), d(x), a(x), \omega\}$ and employ them to provide initial data for our dynamical studies via

$$\phi_i = \frac{\phi}{\cos^2 x}\delta_i^1, \tag{4.1}$$

$$\Phi_i = \frac{\phi'}{\cos x}\delta_i^1, \tag{4.2}$$

$$\Pi_i = \frac{\omega\phi e^d}{a}\delta_i^2, \tag{4.3}$$

where the metric functions are obtained by solving the constraints. We confirm convergence of the obtained solutions (by monitoring the constraint residuals, charge and mass conservation and self-convergence vs time) as resolution is increased (see also [13]).

A. Perturbed, genuine boson stars

We concentrate on studying the behavior of these solutions when perturbed, and have considered various forms of perturbation with qualitatively similar results. For concreteness, we here present results obtained with Gaussian perturbations parametrized as $G(x) = \epsilon e^{-(r-R_0)^2/\Delta^2}$ and add it to the boson star solution via

$$\phi_i = [\phi/\cos^2 x + G(x)]\delta_i^1, \tag{4.4}$$

$$\Phi_i = [\phi'/\cos x + G'(x)]\delta_i^1, \tag{4.5}$$

$$\Pi_i = [\omega\phi(e^d/a) + G']\delta_i^2. \tag{4.6}$$

In analogy with previous studies, we set the amplitude of the Gaussian perturbation to ϵ. We note that because the constraints are solved numerically at the initial time for $a(x, 0)$ and $\delta(x, 0)$, this perturbed initial data together with the obtained metric variables is fully consistent with the equations of motion. Because our numerical implementation is fully non-linear, it naturally probes the nonlinear behavior of this system, and we are particularly interested in the stability of these boson star solutions.

Recall that Ref. [9] found that pulses of scalar field in AdS are unstable to black hole formation, and subsequent arguments in [8] supported this view of generic instability. A reasonable expectation in light of those works is that any perturbation of the boson star will behave in a similar way; that is, one expects such a perturbation to travel back and forth between origin and AdS boundary, sharpening with

each pass, leading eventually to BH formation. However, our early studies suggested quite the opposite (for sufficiently small perturbations); that instead boson stars were stable [17] prompting us to study this system more broadly and deeply.

For small perturbations, very long-lived, regular solutions were obtained describing perturbed boson stars. For such long-lived solutions, we monitored the metric functions (e.g. $\max|1 - A(x,t)|$ and $\delta(0,t)$) and they showed no signs of instability to BH formation. These observations prompted a thorough study of the instability in AdS; independent work via perturbative studies also pointed out that AdS should be stable for several families of solutions [7].

A variety of boson star solutions were studied, including members of levels 0, 1, and 3 (level 2 solutions presented regularity issues near the AdS boundary and we defer such analysis for future work). All examples appeared stable. Interestingly, in asymptotically flat scenarios, excited boson stars are generally unstable, radiating energy and settling into a ground state solution [20]. In AdS, however, there is no way to rid itself of excess charge, which presumably explains their stability. Nevertheless, this property of AdS does not explain how the boson star can be immune to the weakly turbulent instability. Below, we present an argument to this end, but first we discuss the behavior of a different family that lends support to our argument.

B. Fake boson stars

Of course numerical evolutions are limited to finite times, and so one cannot rule out that instability will manifest after the code has been stopped or beyond the time for which one trusts the results. To better assess the observed behavior, we compare these long-lived solutions to a different family which can be considered "nearby" in some sense. This family, which we refer to as fake boson stars, represents purely real initial data with the same mass and profile as their counterpart genuine boson stars. A fake counterpart of some boson star solution of (4.3) is achieved via the transformation,

$$\phi_1^{\text{fake}} = \phi_1^{\text{BS}}, \qquad \Pi_1^{\text{fake}} = \Pi_2^{\text{BS}}, \qquad \Pi_2^{\text{fake}} = 0. \tag{4.7}$$

Remarkably, the evolution of this family also yields regular, long-lived solutions for small perturbations that do not collapse to a black hole. Figs. 5 and 6 illustrate the time of collapse as a function of ϵ both for genuine and fake boson stars. As indicated in the figures, successively higher resolutions largely coincide with differences only apparent at the latest times. In all cases, the results indicate collapse times increasing quickly as ϵ decreases with no signs of collapse for smaller amplitudes of perturbation.

Notice that these fake solutions are not stationary and have no charge, two seemingly essential features of genuine boson stars, and so their apparent immunity to this weakly turbulent instability is surprising. This "stability"

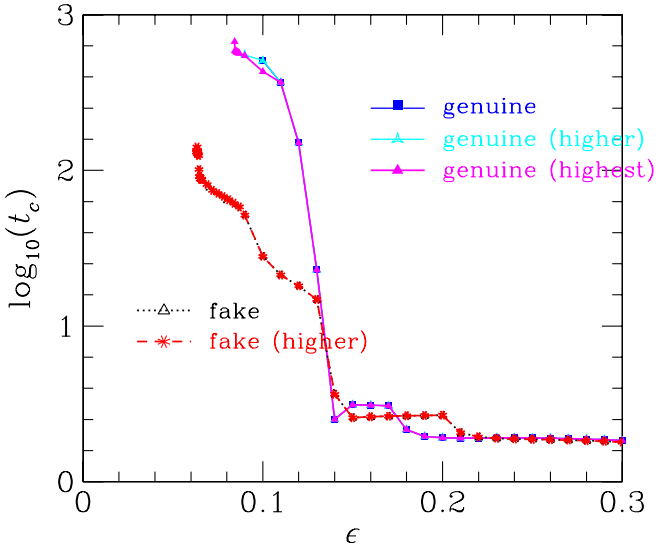

FIG. 5 (color online). Collapse times for Gaussian perturbations of a ground state boson star ($\phi_1(0,0) = 0.253$) and its corresponding fake star. Increasing resolutions are shown. For short collapse times, resolutions agree. However, for the longest evolutions, higher resolutions are needed. Even with very high resolutions, small ϵ evolutions show no sign of collapse.

is apparently not tied to special features (e.g. charge or stationarity) but instead suggests that the dynamics undergoes something akin to a frustrated resonance in which amplitudes increase at times but then disperse. In particular, one essential aspect common to both genuine and fake boson stars appears to be their noncompact, long-wavelength nature. Because they have energy distributed

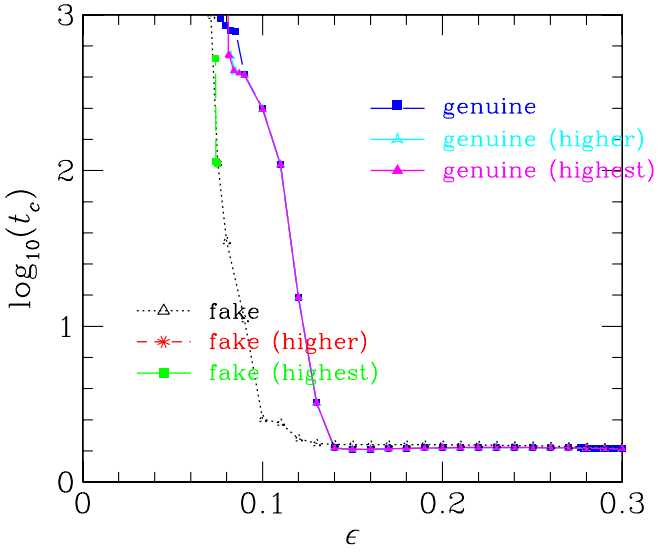

FIG. 6 (color online). Collapse times for Gaussian perturbations of a first excited state boson star ($\phi_1(0,0) = -0.272$) and its corresponding fake star. As in Fig. 5, higher resolutions are also shown with differences among the resolution appearing only at very late times.

throughout the domain, modes no longer propagate coherently. Instead there is a continuing competition between dispersion and gravitational contraction; collapse to a black hole or not is then determined by the outcome of this competition.

C. Large σ

Admittedly, this argument is far from rigorous. But if it holds, then it would imply many other forms of stable initial data. In particular, perhaps other forms of initial data may be immune to this weakly turbulent instability when its extent is large. To explore this conjecture, we adopt the same form of data considered in many previous studies of this instability (such as those in [9,13,19,21,22]). We thus consider this family again, which takes the following form in our rescaled variables:

$$\Phi_i(0,x)=0, \qquad \Pi_i(0,x)=\frac{2\epsilon}{\pi}e^{-\frac{4\tan^2 x}{\pi^2\sigma^2}}\cos^{1-d}x\,\delta_i^1. \quad (4.8)$$

To test the possibility of regular development of this data, we considered the time development of Eq. (4.8) with varying values of σ. The results are plotted in Figs. 7 and 8 which show the time of collapse as a function of ϵ for various values of σ. As is evident from the figures, for small values of σ ($\sigma<0.3$) the collapse time increases monotonically as ϵ decreases; however for larger values of

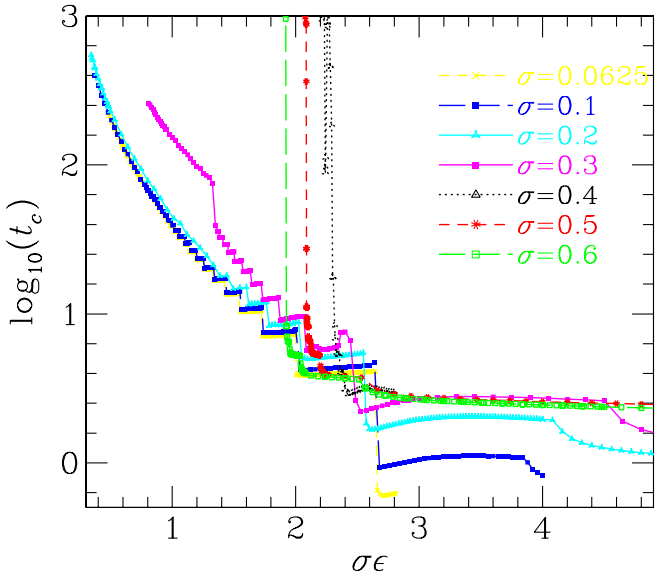

FIG. 7 (color online). Collapse times for initial data of the form Eq. (4.8) with varying width values, σ. Because changes to σ affect the amount of mass, the natural parameter against which to plot is $\sigma\epsilon$ not just ϵ (also see Fig. 8 for this data plotted versus ϵ). Note that for $\sigma \lesssim 0.3$ the standard behavior is observed where collapse eventually occurs for any ϵ. In contrast for $\sigma \gtrsim 0.3$, there appears to exist a threshold ϵ^* below which collapse does not occur. For initial data above the transition, $\sigma > 0.3$, evolutions with smaller ϵ than shown reached at least $t \approx 2000$ with no signs of eventually collapse.

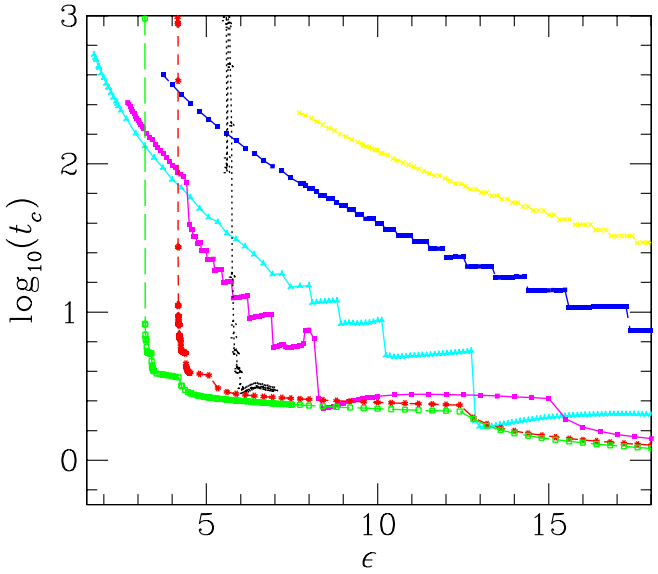

FIG. 8 (color online). Same data as Fig. 7 but with an unrescaled abscissa. As one's eye moves from upper right down to lower left, the initial data parameter σ increases and the behavior of the time of collapse, t_c, changes dramatically from the "usual" stair-step to something else entirely with a very sharp transition. Note that the spacing between runs is very nonuniform and that tuning is necessary to resolve the transition.

σ the collapse time increases abruptly as ϵ is decreased. Notice that this abrupt growth in collapse time behaves quite similarly to that seen for boson stars and fake stars, suggesting that for sufficiently large σ, the behavior would be regular. Furthermore, an analysis of the Fourier power spectra of cases below $\sigma \approx 0.3$ reveals that the spectra monotonically shift to higher frequencies as time progresses. In contrast, for cases above $\sigma \approx 0.4$, they do not do so. Instead the shift saturates and the spectral content oscillates within a narrow window of frequencies.

That large-σ initial data are immune to the weakly turbulent instability is consistent with the argument that widely distributed mass energy prevents the coherent amplification typical of the instability. It is interesting to consider what would happen in the semilinear wave equation on a fixed AdS background as studied in [22]. That model shows many of the same characteristics as the gravitating scalar collapse, but the nonlinear potential plays the role of the attractive, focusing effect that gravity plays here. However, numerical evidence from that model suggests that there is no large-σ effect, lending support to the idea that the distributed mass energy affects the spacetime in a way that disturbs the coherent amplification.

A change in behavior such as this merits a closer examination of the "transition region" between apparent stability and black hole collapse. Figure 9 illustrates this region $0.3 \leq \sigma \leq 0.4$ in more detail. Interestingly, in this transition region, the time-to-collapse exhibits a seemingly oscillatory behavior prior to displaying the characteristic rapid growth as ϵ is decreased.

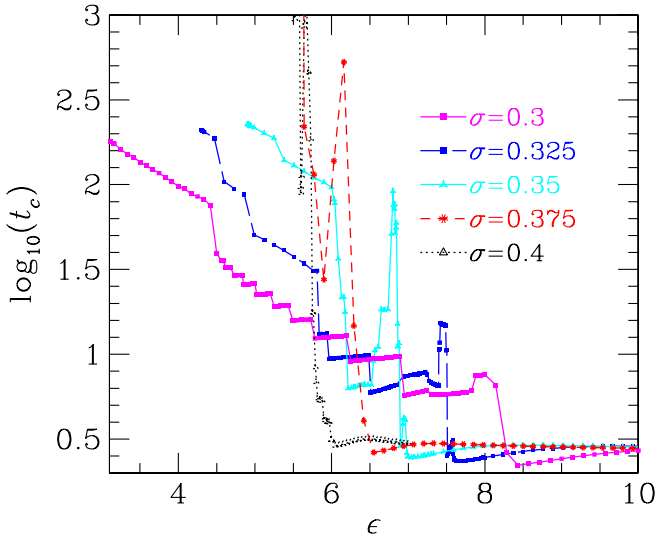

FIG. 9 (color online). Collapse times for a range of σ that demonstrates the transition from turbulent BH formation to frustrated resonance. For $\sigma = 0.3$, collapse appears inevitable for any value of ϵ in contrast to the results for $\sigma = 0.4$. Interestingly, a "bump" appears for these values of σ in which the collapse times demonstrate a lack of monotonicity. Beginning with $\sigma = 0.3$ (magenta, solid squares) around $\epsilon \approx 8$, one sees a small bump that, as one looks to higher σ, sharpens and occurs at smaller ϵ values.

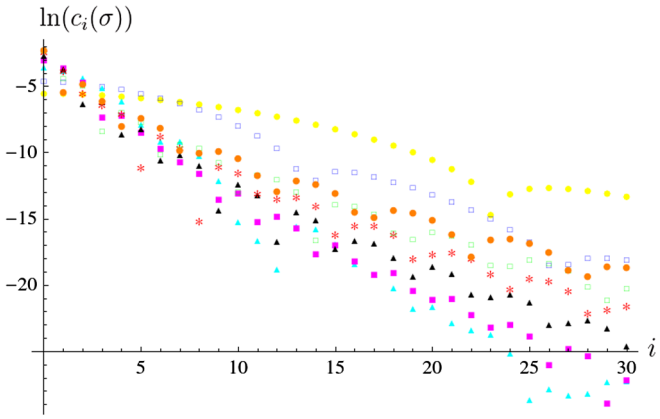

FIG. 10 (color online). Spectral decomposition of the initial data (4.8) with $\sigma = \{0.0625, 0.1, 0.2, 0.3, 0.4, 0.5, 0.6, 0.7\}$ (yellow circles, blue squares, cyan triangles, magenta squares, black triangles, red stars, green squares, orange circles) and $\sigma\epsilon = 1$ in the oscillon basis. Spectral coefficients $c_i(\sigma)$ [see (4.9)] start relatively large at high oscillon numbers for $\sigma = \frac{1}{16}$ (circles); they decrease for $\sigma = 0.1$ (squares), and achieve a minimum profile around $\sigma = 0.2$ (triangles) or $\sigma = 0.3$ (squares); then they increase for $\sigma = 0.4$ (triangles), $\sigma = 0.5$ (stars), $\sigma = 0.6$ (squares) and $\sigma = 0.7$ (circles). The minimum of the spectral coefficient profile roughly coincides with the critical value of $\sigma \sim 0.2$–0.4, which separates stable and unstable regions in the parameter space of the initial data (4.8).

From Figs. 7 and 9, it is clear that for $\sigma \geq 0.4$ there is some $\epsilon_{\min}$ below which initial data does not form a black hole. The idea of this function $\epsilon_{\min}(\sigma)$ is similar to $\epsilon_{\min}(x_{\max})$ studied in [22]. Preliminary study of $\epsilon_{\min}(\sigma)$ shows it to be a roughly exponentially decreasing function (after the apparent discontinuity at $\sigma \approx 0.4$ in which $\epsilon_{\min} = 0 \rightarrow 5.6$). The behavior below $\epsilon_{\min}$ is demonstrated in Fig. 11. In particular, for this weak initial data when the metric is frozen at its initial profile, the evolution demonstrates dispersion.

It is instructive to study the spectral decomposition of the initial data (4.8) in the oscillon basis for different σ. To relate with the analysis in Fig. 7, we keep $\sigma\epsilon = 1$ fixed. For a select set, i.e., $\sigma = \{0.0625, 0.1, 0.2, \ldots 0.7\}$, we compute the spectral coefficients $c_i(\sigma)$, see (2.5),

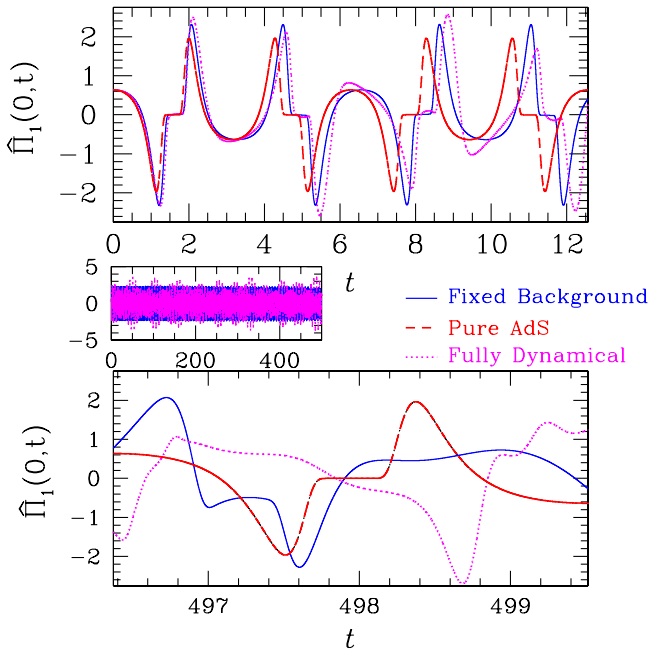

FIG. 11 (color online). Demonstration of dispersion introduced by widely distributed mass energy. Shown is the behavior of Π at the origin during the evolution of $\epsilon = 1$, $\sigma = 1$ initial data. By keeping $A = 1$ and $\delta = 0$, we evolve the scalar field in a pure AdS background, and this results in a periodic solution (dashed, red line). Instead, by solving for the initial metric $A(x, 0)$ and $\delta(x, 0)$, we evolve the scalar field on a fixed background (solid, blue line). This fixed-background evolution displays the dispersion introduced by the fixed metric. The fully dynamical evolution (dotted magenta) is also shown. In the intervening time (see inset), this solution shows the periods of focussing and dispersal typical of what we call frustrated resonance. Finally, at late times, we copy the pure AdS solution from the period $0 < t < \pi$ and display it shifted in time (dot-dashed black); that it overlays the pure AdS solution shows that scalar solutions on a background of AdS are periodic. This figure is similar to Fig. 5 of [22] which shows the dispersion introduced by a restricted domain.

$$c_i = \left| \frac{1}{\omega^{(i)}} \int_0^{\pi/2} dx \tan^2 x A(0,x) e^{-\delta(0,x)} \Pi_1(0,x) e_i(x) \right|, \tag{4.9}$$

where $A(0,x)$ and $\delta(0,x)$ are obtained from integrating (2.8) with initial data (4.8). The resulting spectral decompositions are collected in Fig. 10. Comparing with the spectral decomposition of boson stars (see Fig. 3), here, the large-j decay of the spectra is approximately exponential, instead of a power law as in (3.29). The spectral profile achieves a minimum around $\sigma \sim 0.2$–0.4, which is roughly the critical value of σ separating the stable and unstable regions in the parameter space of the initial data (4.8).

D. Restricted domain

The last nonlinear effect presented in this section concerns evolutions conducted in a restricted domain. In particular, an artificial, reflecting boundary condition is applied at some $x_{\max} < \pi/2$, restricting the propagating pulse to some subdomain of AdS. The motivation for this is to study whether this turbulent instability is itself just the manifestation of the nonlinear attraction of gravity occurring in a bounded domain, or instead some particular property of the full AdS (and hence would be destroyed by this restriction).

As found in [13], the imposition of such a reflecting boundary condition does not eliminate black hole formation after multiple bounces. However, a minimum value of ϵ was found, below which no such black hole formation occurred. In the semilinear model, it was found that the boundary condition resulted in dispersion not seen with the full AdS domain.

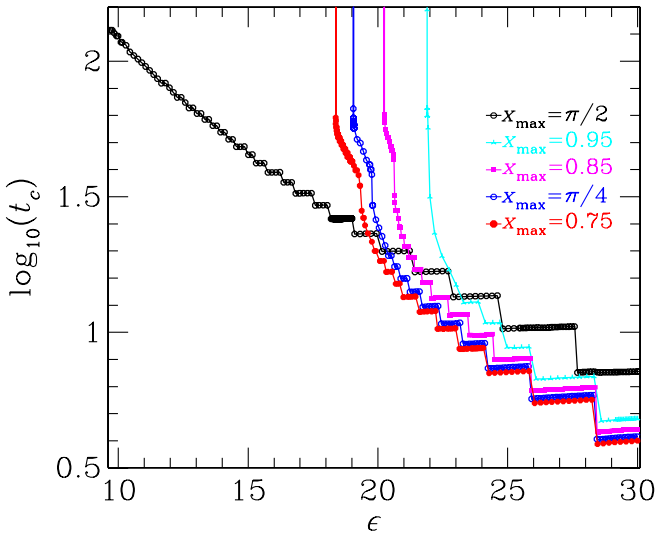

FIG. 12 (color online). Collapse times of the initial data in Eq. (4.8) with $\sigma = 1/16$ with an artificial, reflecting wall at a various positions, $x_{\max}$. Also shown (solid black) are the results for the full domain with no reflecting wall. Note that the finite domain evolutions demonstrate a threshold $\epsilon_{\min}$ below which collapse does not occur.

Here, we revisit this problem, showing the customary time of collapse plot in Fig. 12. As mentioned, there is some similarity with the large-σ effect in the existence of some $\epsilon_{\min}$. However, in contrast, one does observe the "stair-step" decrease in collapse time for ϵ increasing above $\epsilon_{\min}$, characteristic of successive bounces.

It is also possible that such restricted-domain evolutions result from the following two effects: (i) the imposition of the reflecting wall introduces dispersion as in the semilinear model, and (ii) as the domain shrinks, there may be some effect due to the fact that, for fixed σ, the fractional support of the initial data is increasing.

V. CONCLUSIONS

We have constructed boson star solutions in global AdS and shown that they are stable at linear order. Numerical studies of their dynamics strongly suggest that these boson stars, both ground state and the first few excited states, are nonlinearly stable. Along with solutions presented in [15], there is now considerable evidence that the instability of AdS to scalar perturbations reported in [9] is limited in scope, that there exist nontrivial, dynamical examples of stable solutions in AdS. These results are consistent with the perturbative arguments of [7] for the stability of boson stars, geons and solitons.

Comparison of the lifetimes of perturbed boson stars with other, nonstationary solutions, our fake boson stars, reveals an even wider class of initial data which appears to frustrate the resonance and thereby avoid collapse for sufficiently small amplitude. Indeed, using the very same family of the seminal work of [9], numerical evolutions suggest that for initial data with $\sigma \gtrsim 0.4$, the instability can be avoided. More generally, initial data with widely distributed mass energy appears to be similarly immune to the turbulent instability. This behavior is in contrast to what is observed in solutions to the semilinear wave equation in (flat) AdS. There, a singularity always forms [22], even for large-σ, indicating that gravity plays a key role in the dynamics. In particular, a heuristic argument suggests that the widely distributed mass energy distorts the space sufficiently to introduce dispersion and thereby oppose the concentrating effect of the instability.

The picture that emerges is a phase space with (at least) two regions. One region is subject to the weakly turbulent instability and therefore collapses for any initial "amplitude." The other region can avoid the turbulent instability and contains oscillons, boson stars, geons, and similar symmetric solutions. However, it appears this second "stable" region contains a wider class of solutions with no periodicity or stationarity, namely fake boson stars, large-σ and similarly distributed families of initial data. To be clear, this second region need not be strictly stable and can certainly possess collapsing solutions. What is

important is that in this second region, one can choose a sufficiently small amplitude such that the weakly turbulent instability is avoided.

We do not know at this stage the precise criterion that separates the parameter region of scalar field initial data resulting in BH formation from the region of nonlinear stability. It can be argued that such a criterion is encoded in the spectral decomposition of the initial data in the oscillon basis. Indeed, consider the region (assuming it exists[8]) where collapse occurs for arbitrarily small amplitude of the scalar field. In this limit, the full initial data is the oscillon spectrum, as the backreaction can be safely ignored. In this paper we presented strong evidence for initial configurations that do not collapse in the limit of vanishingly small amplitude. Thus, the distinction between stable and nonstable configurations (at least for small amplitudes) must be hidden in the initial scalar field spectral data. We have seen that initial profiles of [9] (4.8) become stable for small ϵ as σ increases; the latter increase results in softening the decay of the asymptotic oscillon spectral coefficients (see Fig. 10). Likewise, boson stars have an asymptotic power-law oscillon spectral decomposition, in contrast to the exponential-decay profile for initial data (4.8) (see Fig. 3).

It is important to further investigate the nonlinear stability of AdS. The issue has profound implications for a dual boundary conformal field theory, as it identifies CFT initial configurations that fail to thermalize. There is no obvious symmetry criterion "protecting" such configurations. A possible future direction is to investigate the collapse of initial configurations specified by their oscillon spectral decompositions with various trial profiles c_i. The primary goal, of course, is the identification of the stability criteria—it is possible that the latter can be established from analysis of the weakly nonlinear regime only. Finally, it is interesting to analyze the stability of more general configurations, such as boson stars with local bulk charge, as recently discussed in [23–25].

[8]Numerical analysis of [9] strongly supports that this is the case.

ACKNOWLEDGMENTS

It is a pleasure to thank Oscar Dias, Chad Hanna, Gary Horowitz, Pavel Kovtun, Robert Myers, Andrzej Rostworowski and Jorge Santos for interesting and helpful discussions. This work was supported by the NSF (PHY-0969827 to Long Island University) and NSERC through Discovery Grants (to A. B. and L. L.). For hospitality, L. L. and S. L. L. thank the KITP, where parts of this work were completed. Research at Perimeter Institute is supported through Industry Canada and by the Province of Ontario through the Ministry of Research & Innovation. Computations were performed thanks to allocations at the Extreme Science and Engineering Discovery Environment (XSEDE), which is supported by National Science Foundation Grant No. OCI-1053575 as well as SHARCNET.

[1] O. Aharony, S. S. Gubser, J. M. Maldacena, H. Ooguri, and Y. Oz, Phys. Rep. **323**, 183 (2000).
[2] A. Ishibashi and K. Maeda, Phys. Rev. D **86**, 104012 (2012).
[3] G. Holzegel, arXiv:1103.0710.
[4] G. Holzegel and J. Smulevici, Commun. Math. Phys. **317**, 205 (2013).
[5] G. H. Holzegel and C. M. Warnick, arXiv:1209.3308.
[6] G. Holzegel and J. Smulevici, arXiv:1303.5944.
[7] O. J. Dias, G. T. Horowitz, D. Marolf, and J. E. Santos, Classical Quantum Gravity **29**, 235019 (2012).
[8] O. J. Dias, G. T. Horowitz, and J. E. Santos, Classical Quantum Gravity **29**, 194002 (2012).
[9] P. Bizon and A. Rostworowski, Phys. Rev. Lett. **107**, 031102 (2011).
[10] P. M. Chesler and L. G. Yaffe, Phys. Rev. Lett. **106**, 021601 (2011).
[11] D. Garfinkle and L. A. P. Zayas, Phys. Rev. D **84**, 066006 (2011).
[12] H. Bantilan, F. Pretorius, and S. S. Gubser, Phys. Rev. D **85**, 084038 (2012).
[13] A. Buchel, L. Lehner, and S. L. Liebling, Phys. Rev. D **86**, 123011 (2012).
[14] M. Chernicoff, D. Fernandez, D. Mateos, and D. Trancanelli, J. High Energy Phys. 08 (2012) 041.
[15] M. Maliborski and A. Rostworowski, arXiv:1303.3186.
[16] M. W. Choptuik, Phys. Rev. Lett. **70**, 9 (1993).
[17] S. L. Liebling, Exploring AdS/CFT Dualities in Dynamical Settings, Perimeter Institute, 2012, http://pirsa.org/12060023.
[18] D. Astefanesei and E. Radu, Nucl. Phys. **B665**, 594 (2003).
[19] J. Jalmuzna, A. Rostworowski, and P. Bizon, Phys. Rev. D **84**, 085021 (2011).
[20] S. L. Liebling and C. Palenzuela, Living Rev. Relativity **15**, 6 (2012).
[21] M. Maliborski, Phys. Rev. Lett. **109**, 221101 (2012).
[22] S. L. Liebling, Phys. Rev. D **87**, 081501(R) (2013).
[23] S. A. Gentle, M. Rangamani, and B. Withers, J. High Energy Phys. 05 (2012) 106.
[24] S. Hu, J. T. Liu, and L. A. P. Zayas, arXiv:1209.2378.
[25] Y. Brihaye, B. Hartmann, and S. Tojiev, Classical Quantum Gravity **30**, 115009 (2013).